Heat Transport in Photothermal Microscopy: Newton vs Fourier

Panagis Samolis,[†] Mi K. Hong,[‡] R. Rajagopal,[‡] Michelle Y. Sander,*,[†] Shyamsunder Erramilli ,*,[‡] and Onuttom Narayan*,[¶]

†ECE department, Boston University, 15 St Mary St, Boston, MA-02215, USA ‡Physics department, Boston University, 590 Commonwealth Ave, Boston, MA-02215, USA ¶ Physics Department, University of California, Santa Cruz, CA 95064

E-mail: msander@bu.edu; shyam@bu.edu; onarayan@ucsc.edu

Abstract

Technological breakthroughs in photothermal microscopy have led to new discoveries in thermal transport at the cellular level. In the linear regime, heat transport is governed by the well-understood parabolic partial differential heat equation and its many extensions with antecedents dating back to Fourier. The relaxation of the temperature from a point impulsive source of heat in a homogeneous medium in d dimensions is scale free and asymptotically follows a power law decay in time $\sim t^{-d/2}$. It is therefore interesting that many recent experiments have used Newton's law of cooling, an ordinary differential equation that yields exponential decays with a single time constant. We show that the observed apparent exponential decays in photothermal microscopy are set by externalities such as the sample cell design, experimental finite excitation pulsewidth and spatial resolution and should still contain a power law pre-factor. Combining analytical methods that include exact results and asympototic analysis with experiments and numerical simulations, we show that the conditions for

the emergence of Newton's law of cooling are often not satisfied in experiments. These need to re-interpreted to be consistent with the underlying Fourier theory at the microscopic sub-cellular length scales, taking into consideration the Interfacial Thermal conductance or equivalently the inverse Kapitza resistance at interfaces.

Introduction

In photothermal microscopy in condensed phases, a focused pump laser pulse is resonantly absorbed, forming a localized microscopic heat source $q(\mathbf{r}', t')$. The consequent temperature rise changes the local optical properties forming what has been historically called a 'thermal lens', which is detected by elastic scattering of a probe laser tuned off resonance. About twenty years ago Berciaud et al, presented a systematic analysis of photothermal microscopy in a homogeneous medium. They started with the Fourier heat partial differential equation (PDE) to describe the time evolution of the temperature field $T(\mathbf{r}, t)$ in response to a stimulus provided by a heat source q. In a heat conducting medium with an intrinsic material thermal diffusivity D, the temperature field is described by the equation to the left:

$$\frac{\partial T(\mathbf{r},t)}{\partial t} = D\nabla^2 T(\mathbf{r},t) + q(\mathbf{r},t) \quad \stackrel{?}{\leftrightarrow} \quad \frac{dT}{dt} = -h(T-T_0) + q(t) \tag{1}$$

In the linear regime, as is well known from the Einstein-Smolochowski analysis, the temperature change in Fourier theory decays in a scale-free manner: $\Delta T \sim t^{-d/2}$. The exponent in the power law dependence in this expression is set by the spatial dimensionality d. The self-similar nature of the decay is evident by the absence of any temporal scale parameter in the non-equilibrium dynamics initiated by a delta function impulse heat source. Formally, the heat equation is the Schrödinger equation for a free particle in imaginary time. There are no discrete eigenvalue solutions, and hence there is no single time constant that describes the time evolution. The PDE may be contrasted with Newton's law of cooling described by an *ordinary* differential equation (ODE) shown on the right of Eq.(1). Newton's law of cooling leads to a single exponential relaxation.

Several groups around the world³⁻⁶ have described systematic experiments in concert with finite element method simulations of the Fourier heat equation that support the original description² in the linear regime. We have recently extended this established analysis both analytically and computationally to the case of a biological membrane that separates a medium into two topologically disconnected regions.⁷ In a linear dielectric medium with small changes in temperature, the change in the dielectric susceptibility is given by $\delta \epsilon(\mathbf{r},t) = \gamma dT(\mathbf{r},t)$ neglecting non-local effects, where γ is a thermo-optic material constant of the medium (in water $\gamma \approx 1.4 \times 10^{-4} \mathrm{K}^{-1}$). Given the temperature field solution of the heat equation, the differential scattering cross-section of the probe laser in the first Born approximation⁷ is given by the expression:

$$\frac{d\sigma}{d\Omega} = \frac{k^4}{(4\pi\epsilon_0)^2} \left| \int d\mathbf{r} \exp[i(\mathbf{k}_{in} - \mathbf{k}_{out}) \cdot \mathbf{r}] \mathbf{e}_{out}^* \cdot \mathbf{e}_{in} \delta\epsilon(\mathbf{r}, t) \right|^2$$
(2)

In the weak linear regime the first Born approximation expressions are equivalent to those obtained in the Rytov approximation that has become increasingly popular in the microscopy community, both in the forward and back-scattering imaging modes in systems with smooth optical phase gradients that determine image contrast. The central widely accepted principle² is that the detected elastic scattering photothermal signal in a condensed phase arises from the thermally induced change in the optical properties of the surrounding medium, and not primarily from changes in the underlying refractive index of any nanoparticle absorber that may be used in experiments to approximate the point source.

Interpreting thermal decay: Over the past several years, it has become common in the field of photothermal microscopy to hark back to the much earlier insight of Newton. The time evolution of the temperature is assumed to obey an ODE, neglecting any potential continuous spatial variation. Newton's great insight holds when heat is transferred to an infinitely large environment maintained at a fixed temperature T_0 no matter how much heat

is absorbed. This idealization is appropriate either when there is significant convection or in a medium with an effectively infinite heat capacity. The temperature T(t) in the system relaxes exponentially in time to the reach the equilibrium heat bath temperature T_0 with the transport described by a phenomenological heat transfer coefficient h. Newton's law has been uncritically applied in aqueous media for local temperature relaxation far from any solid crystalline substrates, and even at the sub-cellular level with negligible convection (see Song et al⁸ and references therein). Beyond the field of photothermal microscopy, the single exponential thermal relaxation description has been used in photoacoustic relaxation experiments in polymers⁹ to measure the thermal diffusivity of the medium. And indeed, many photothermal experiments that have limited dynamic range do appear to show thermal decays that superficially "look exponential" (Figure 1c). The observed exponential decay time constant τ_m is argued to be inversely proportional to the thermal diffusivity $\tau_m \propto 1/D$ of the medium, independent of particle morphology and sample thickness and irrespective of the mechanism of heat transport.¹⁰

Our goal in this note is to reconcile these two descriptions and to point out some dangers in interpreting experimentally observed time constants given the scale-free nature of the Green's function of the underlying Fourier heat equation. There is a need for a rigorous description in light of rapid and impressive experimental advances in photothermal microscopy and quantitative phase imaging enabled by new imaging instrumentation with sub-microsecond resolution $^{11-14}$ by groups around the world, $^{4,15-17}$ and in plasmonic enhancement methods 18,19 that have enabled fast widefield microscopy 8 with potential for single shot studies. With the development of AFM-based photothermal microscopy, 20 direct nanoscale measurements have been enabled on the ≈ 35 nm scale of the interfacial thermal conductance and thermal conductivity.

A few comments are pertinent. It is well known that Newton's law of cooling can emerge in specific geometries when advection is significant in systems with experimental boundary conditions at a sufficiently small Biot number or a sufficiently large Nusselt number where the

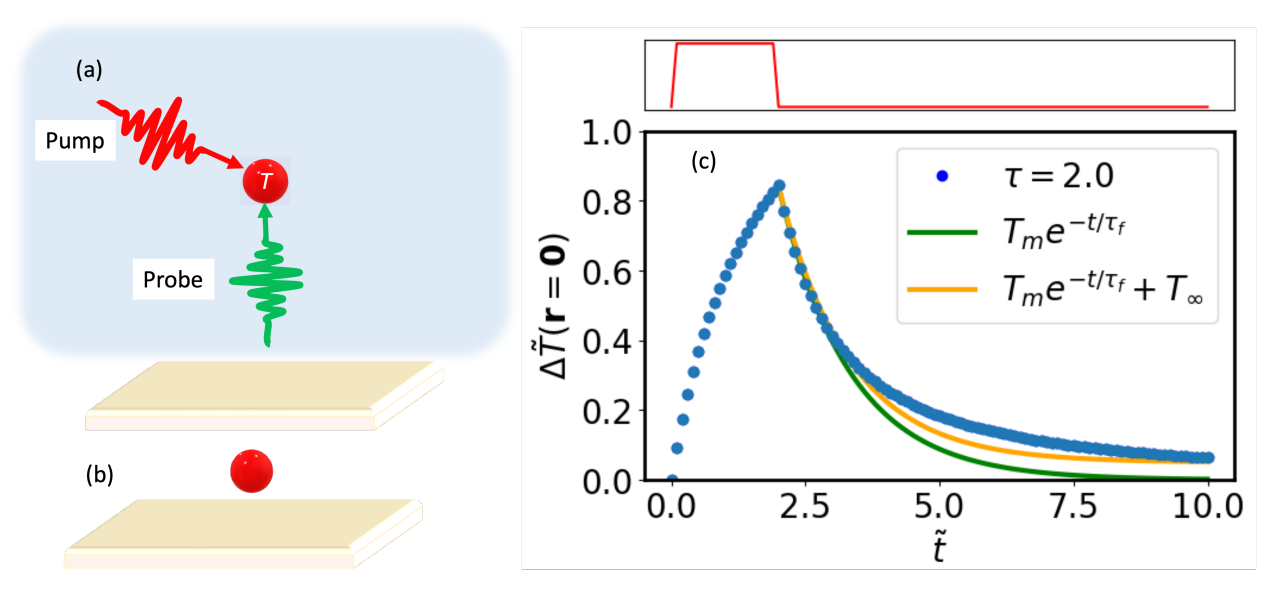


Figure 1: Heat transport in an aqueous medium from a point source experimentally realized by a nanoparticle that is resonantly excited by a pulsed pump laser with a rectangular temporal shape. (a) Heat transport governed by the Fourier 3D diffusion heat equation and (b) Thin film geometry of a nanoparticle sandwiched between two crystalline substrates. (c) Solution of the Fourier equation in a homogeneous medium with a spatial Gaussian pump laser pulse (dots) with the rectangular temporal profile shown on top, as described in the text (Case 1). The solid green line is a single exponential decay that misses the long time tail. The solid orange line adds an offset that never decays back to equilibrium. The data can indeed 'look' deceptively like a single exponential - either with and without an offset but the rise and fall time-scales are set by the temporal duration of the pump laser rather than any intrinsic transport properties of the aqueous medium.

ODE description may indeed be appropriate. 12 An example is a series of experiments 12,21 in which polystyerene and PMMA nanoparticles of varying sizes were spincoated onto a Calcium Fluoride window in air and photothermally excited by a mid-infrared laser tuned to selected IR active molecular vibrations. The Nusselt number for air surrounding nanoparticles was estimated to be $\simeq 2^{12}$ in support of the idea that conductive heat transfer is somewhat more important than convection. The authors argued that they could ignore conductive heat transfer from the nanoparticle to the crystalline substrate even though CaF₂ is an excellent conductor of heat, because of the negligible contact area and the limited range of intermolecular forces. 21 Under these assumptions, the far simpler Newtonian two-temperature model would then be sufficient since the relaxation is dominated by heat transfer to air, 12 which was assumed to equilibrate infinitely quickly with the substrate, even on the fast 10 of nanosecond time-scales of the pump laser pulse dureations. The observed exponential relaxation of the measured photothermally induced contrast in time was interpreted as being due to elastic scattering arising from thermally induced changes in the refractive index of the nanoparticle in the Lorenz-Mie or Rutherford regimes, rather than in the surrounding embedding medium of air.

By contrast, Ishigane et al⁶ studied $10\mu\text{m}$ thin liquid samples restricted by the very large extinction coefficient from the OH stretch vibration and large $\approx 90\mu\text{m}$ focal spots of a midinfrared pump laser. The thermal transport is dominated by contact with the CaF₂ windows that have a thermal conductivity $\kappa_C \approx 9.7\text{W} \cdot \text{m}^{-1} \cdot \text{K}^{-1}$ about 16 times greater than water $\kappa_w \approx 0.6\text{W} \cdot \text{m}^{-1} \cdot \text{K}^{-1}$, with the relaxation fit to a single exponential in time. In Section III, we derive the exact appropriate 3D Green function for this sandwich thin film geometry which includes a power law pre-factor with an infinite series of discrete exponential functions. We show that a single term can dominate in selected experimental geometries. Apart from the power-law pre-factor that is missing in these prior reported experimental analyses, we show that the exponential time-scale observed rather depends very strongly on the geometry and the thickness of the sample film. In Section IV we address the homogeneous case, where

the discrete exponentials are replaced by a pure power-law decay. Even here, we show that there can be apparent 'exponential' decays, where the decay time constant now depends on the laser pulse characteristics and finite size effects or even the transfer functions associated with electronic filters in AC-coupled experiments.

Interfacial Thermal Conductance. In a recent article in 2022 Chen et al²² reviewed fundamental theories and challenges, and traced the history of Interfacial Thermal Resistance (ITR). Kapitza in 1941 noticed a large temperature difference ΔT between a Copper heater and superfluid Helium in contact with the heater. Careful studies of sample thermalization revealed that almost the entire temperature drop occurred in a very thin idealized boundary layer. It was then permissible to define a thermal interfacial boundary resistance, a 'lumped' thermal circuit element now called the Kapitza resistance $R_K \equiv 1/G_K = \Delta T/Q$ where Q is the heat flux per unit area of the interface. The corresponding thermal conductance G_K is the more natural quantity of interest. In recent years, the terms "Interfacial Thermal Resistance" and "Kapitza Resistance" have begun to be used interchangeably, although ITR is more general, and the corresponding term "Interfacial Thermal Conductance" is preferred.

Limitations: The note here primarily addresses the question of thermal relaxation at the cellular length scales in liquids and especially aqueous media in the linear regime. At the much larger tissue level, we note that there are well-developed bioheat transfer models, where the presence of vasculature in living tissue leads to hybrid models that incorporate Newton's Law in tissues that are in immediate contact with blood vessels. Tissues with vasculature can indeed be cooled by flowing blood, and local advection should be included. However, on the cellular and sub-cellular length scales considered here, the Peclet number $Pe \ll 1$ and advection can be ignored. At sufficiently high pump laser flux, we have reported very interesting nonlinear effects associated with phase changes. ²³ A detailed theory of nonlinear photothermal microscopy remains an open question and is beyond the scope of this paper. Our scope in this paper can consequently be regarded rather narrow: given that the theoretical community has settled the scale-free nature of heat transport in linear photothermal

microscopy, what is the origin of the apparent experimentally observed exponential decays in photothermal experiments by a number of groups around the world?

Methods

Photothermal experiments were carried out using previously published protocols. 17,24,25 Briefly, a Quantum Cascade Laser (QCL) laser tunable in a wavenumber range $1500-1750~\rm cm^{-1}$ emitting 500 ns pulses at a repetition rate of 100 kHz served as the pump laser. The pump beam illuminated the sample through a 0.4 numerical aperture (NA) refractive ZnSe objective. Samples were sandwiched between CaF₂ windows separated by calibrated spacers and mounted on a microscope stage. An epi-detection setup is implemented for the probe in which a near-infrared continuous-wave laser diode centered at a wavelength of 980 nm is focused on the sample using an NA = 0.65 objective. The elastically scattered probe beam was sent to a photodetector followed by an amplifier with either DC- or AC-coupling. The photothermal signal was measured either in lock-in detection or in Box-car mode as described elsewhere. 24,26

Results

Thin layer geometry

We first consider a fluid confined between two parallel plates that are separated by a distance L, with the plates held at temperature T_p . We orient our coordinates so that one plate is in the plane z = 0 and the other plate is in the plane z = L. A heating pulse is applied at time t = 0 at the point $(0, 0, z_0)$, where $0 < z_0 < L$. Thereafter, the temperature evolves according to the diffusion equation. This problem can be solved using the method of images, but it is more instructive to find the Green's function directly.

If we define $\tilde{T} = (T - T_p)/T_p$, the normalized difference between the temperature and

the temperature of the plates, then

$$\partial_t \tilde{T} = D \nabla^2 \tilde{T} \qquad t > 0 \tag{3}$$

with the initial condition $\tilde{T}(x, y, z, t = 0) = P\delta(x)\delta(y)\delta(z - z_0)$, where P has units of volume and is an amplitude proportional to the energy deposited by the heating laser pulse. In reality, the temperature immediately after the heating pulse is very high in a very small region; the δ -function is an idealized version of this initial condition.

The xy dependence of the temperature corresponds to free diffusion i.e.

$$\tilde{T}(x,y,z,t>0) = f(z,t)\frac{1}{\sqrt{4\pi Dt}}e^{-x^2/(4Dt)}\frac{1}{\sqrt{4\pi Dt}}e^{-y^2/(4Dt)}.$$
(4)

where we have separated variables, and defined the function f(z,t) to capture the (z,t) dependence. It is easy to verify that if we substitute this form in Eq.(3), then f(z,t) has to satisfy the one-dimensional diffusion equation

$$\partial_t f = D\partial_z^2 f \qquad t > 0 \tag{5}$$

with initial condition $f(z, t = 0) = P\delta(z - z_0)$ and boundary conditions f(0, t) = f(L, t) = 0.

We expand f(z,t) in a complete set of eigenfunctions of the ∂_z^2 operator with the appropriate boundary conditions:

$$f(z,t) = \sum_{n=1}^{\infty} c_n \sin\left(\frac{n\pi z}{L}\right) e^{-Dn^2 \pi^2 t/L^2}.$$
 (6)

The n^2 mode index dependence of the eigenvalues of the ∇^2 operator that leads to the n^2 factors in the exponents will be familiar from the corresponding energy eigenfunctions for the Schrödinger equation for a particle confined in a box (SI). We now show that this dependence is important to understand how a single eigenvalue can dominate.

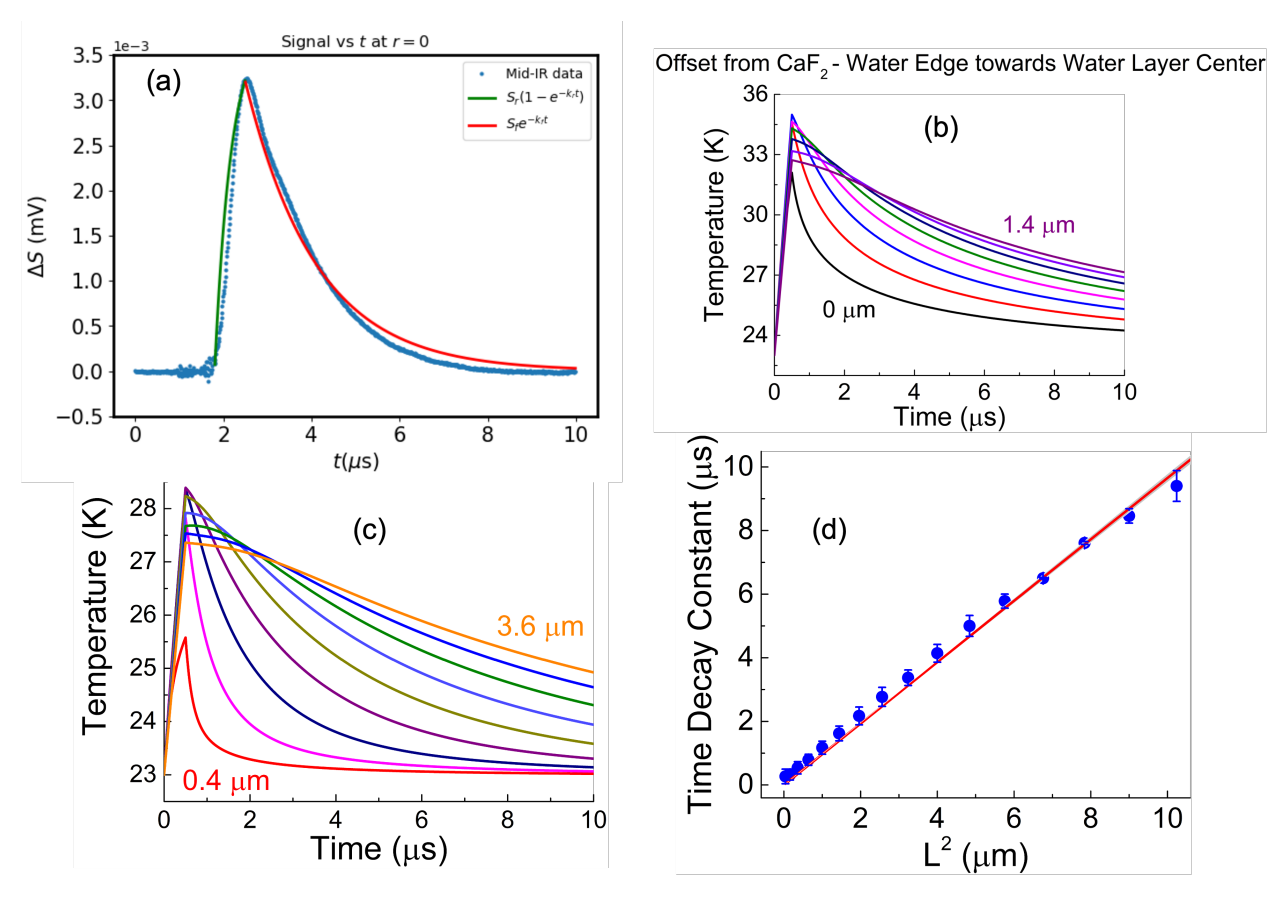


Figure 2: (a) Mid-IR Photothermal data using a Quantum Cascade Laser with AC coupling to block the long time tail in a water film sandwiched between CaF₂ windows. The errors are estimated from the baseline to be 5×10^{-5} or about 1 %. (b) Simulations of rise and fall of temperature initiated by a mid-IR rectangular pump pulse in a thin water film sandwiched between two CaF₂ windows at various distances (increasing in 0.2 μ m from 0 to 1.4 μ m) from the center of the film set as the origin. (c) Finite element simulations of the rise and fall of the temperature at the origin with varying thicknesses L (from 0.4 μ m to 3.6 μ m in 0.4 μ m steps). (d) A characteristic decay time set by the 1/e time of the peak temperature illustrating the L^2 scaling of the dominant eigenvalue λ_1 . While the data "look exponential" during both the rise and falling phase during the rectangular QCL pulse, the analysis needs to be more rigorous to take diffusion into account.

Applying the initial condition, we have

$$f(z,t) = \frac{2P}{L} \sum_{n=1}^{\infty} \sin\left(\frac{n\pi z_0}{L}\right) \sin\left(\frac{n\pi z}{L}\right) e^{-Dn^2\pi^2 t/L^2}.$$
 (7)

Therefore, putting the pieces together,

$$\tilde{T}(x, y, z, t) = \frac{2P}{L} \sum_{n=1}^{\infty} \sin\left(\frac{n\pi z_0}{L}\right) \sin\left(\frac{n\pi z}{L}\right) e^{-Dn^2\pi^2 t/L^2} \times \frac{1}{4\pi Dt} e^{-(x^2 + y^2)/(4Dt)}$$
(8)

The temperature at the point where the heating pulse was applied is then

$$\tilde{T}(0,0,z_0,t) = \frac{P}{2\pi LDt} \sum_{n=1}^{\infty} \sin^2\left(\frac{n\pi z_0}{L}\right) e^{-Dn^2\pi^2 t/L^2}.$$
(9)

When t is large, only the first term in the series survives, and

$$\tilde{T}(0,0,z_0,t>>0) \approx \frac{P}{2\pi LDt} \sin^2\left(\frac{\pi z_0}{L}\right) e^{-D\pi^2 t/L^2}.$$
 (10)

That is, \tilde{T} decays exponentially with time, but with a power law prefactor as a correction.

The biggest term in the series that we have neglected is the n=2 term, which decays four times as fast, as $e^{-4D\pi^2t/L^2}$. However, if the heating pulse is applied at $z_0=L/2$, equidistantly between the plates, then because $\sin(2\pi(L/2)/L)=0$, the biggest term that we have neglected is the n=3 term, which decays nine times as fast as $e^{-9D\pi^2t/L^2}$. Thus, to a good approximation, the decay appears to be dominated by a single exponential. Results from experiments and simulations are shown in Figure 2, using protocols reported in our prior work. The predicted L^2 scaling of eigenvalues is evident for the leading n=1 term in Figure 2(d) even if we do not take the 1/t pre-factor into account that results in a single simple exponential.

In elementary textbooks on heat transport in thin thermal layers, only purely 1D transport is considered and a single exponential is indeed appropriate. The 1/t prefactor we

have derived is a consequence of the 2D nature of transverse diffusion and should not be neglected in photothermal microscopy. Each of the two transverse dimensions contribute a $1/\sqrt{t}$ diffusive factor, combining to a 1/t prefactor. This prefactor will result in the effective exponential decay rate appearing to be slightly larger than what it would be from the exponential factor alone, $D\pi^2/L^2$. Analytical models that fit photothermal data ignore the power law prefactor, but can nevertheless provide reasonable looking fits because of the limited dynamic range in photothermal experiments. The advent of new experimental time-resolved photothermal techniques with greater sensitivity and dynamic range will show these deviations from a simple exponential form in thin film experiments.

Analytical model with open boundary conditions

A number of photothermal studies, particularly those not with mid-IR pump lasers, are performed on thick samples, i.e. the distance over which heat diffuses over the timescales of experimental interest is small compared to the distance from the nanoparticle source to the boundaries of the sample. This is the case for nanoparticle absorbers with resonance in the visible or near-IR regions in aqueous media far from a crystalline substrate. In such a situation, we can approximate the boundaries as being infinitely far away.

The analytic solution to the Fourier heat equation with boundaries at infinity, with a single thermal impulse source at the origin of unit strength that is described by the source term $\delta(\mathbf{r}')\delta(t')$, is the free space Green function G(r,t) which has no space and time scales:

$$G(\mathbf{r} - \mathbf{r}', t - t') = \Theta(t - t') \frac{1}{[4\pi D(t - t')]^{3/2}} e^{-|\mathbf{r} - \mathbf{r}'|^2/4D(t - t')}$$
(11)

Where $\Theta(t-t')$ is the Heaviside step function. The solution for an arbitrary source $q(\mathbf{r}',t')$ is then

$$T(\mathbf{r},t) = \int \int d\mathbf{r}' dt' G(\mathbf{r} - \mathbf{r}', t - t') q(\mathbf{r}', t')$$
(12)

where we have shifted the zero of the temperature scale so that the temperature before the

heating pulse is zero.

If t is large, any small source can be treated as being localized at one point in space and time. The temperature at the location of the source is then $T(\mathbf{r}',t) \propto 1/|t-t'|^{3/2}$. The eigenvalue spectrum for ∇^2 in free space is continuous, which results in this scale-free non-exponential decay. How do we reconcile this with the exponential decay that is reported in many experiments?

Two types of temporal laser pulses are used in experiments. In many phothermal microscopy studies a rectangular pulse is applied, for example from a Quantum Cascade Laser (QCL) in mid-IR microscopy. Pulses with Gaussian envelopes are used in ultrafast laser spectroscopy, and in some Q-switched pump laser systems. The initial spatial distribution is commonly assumed to be uniform over the nanoparticle, although an extension to a profile that varies spatially over the nanoparticle is straightforward from the Green function. The different cases are considered separately.

To simplify our notation, we rescale length and time according to $\ell \tilde{r} \equiv r$, $\zeta \tilde{t} \equiv t$, so that the rescaled diffusion constant $\tilde{D} = D\zeta/\ell^2 = 1/4$ and the rescaled radius of the region the laser pulse is applied to $\tilde{r}_0 = r_0/l$ is unity (see Supplementary Information, SI). This leaves us with the rescaled duration of the laser pulse $\tilde{\tau} = \tau/\zeta$ as a dimensionless parameter. Rescaling the heat source as well $q \equiv Q_0 \tilde{q}$ to de-dimensionalize the description, the temperature at the origin can be obtained by integrating over the Green function:

$$T(\mathbf{r} = 0, t) = Q_0 \zeta \int d\tilde{t}' \Theta(\tilde{t} - \tilde{t}') I(\tilde{t}, \tilde{t}')$$
(13)

This is illustrated in the following cases with explicit expressions for $I(\tilde{t}, \tilde{t}')$ and the resultant time evolution of $T(\mathbf{r}=0,t)$ and thereby the re-scaled dimensionless temperature $\tilde{T}(\mathbf{r}=0,t)$ at the origin.

Case 1: Spatially Gaussian rectangular pulse of duration τ centered in space at the origin. The time evolution of the temperature field at the origin is given by the dimensionless integral that follows from the re-scaled Green function above,

$$I(\tilde{t}, \tilde{t}') = 4\pi \int_0^\infty e^{-\tilde{r}'^2} \frac{e^{-\tilde{r}'^2/(\tilde{t}-\tilde{t}')}}{(\tilde{t}-\tilde{t}')^{3/2}} \tilde{r}'^2 d\tilde{r}'$$
(14)

integrated over $0 < \tilde{t}' < \min[\tilde{t}, \tilde{\tau}]$. We now see that the dimensionless parameter $\tilde{\tau} \equiv \tau/\zeta$ introduced above is the only parameter that quantifies observed time evolution of the temperature during both the rise and fall phases. The spatial integral can now be readily done, leading to the analytical result for the time evolution of the temperature at the origin:

$$I(\tilde{t}, \tilde{t}') = \frac{1}{[1 + (\tilde{t} - \tilde{t}')]^{3/2}}$$
(15)

The time integral $I(\tilde{t}, \tilde{t}')$ over the dimensionless source time \tilde{t}' can also be solved analytically to get the following expressions for the time evolution of the dimensionless scaled temperature at the origin, both during the excitation pulse and over the time course of the evolution after the pump laser turns off:

$$F(\tilde{t}) = \begin{cases} \frac{2}{(1+(\tilde{t}-\tilde{\tau}))^{1/2}} - \frac{2}{(1+\tilde{t})^{1/2}} & \text{if } \tilde{t} > \tilde{\tau} \\ 2 - \frac{2}{[1+\tilde{t}]^{1/2}} & \text{if } \tilde{t} < \tilde{\tau} \end{cases}$$
(16)

The exact algebraic result with the power law functions does not 'look exponential'. It is well known in the glass transition, chemical kinetics and quantitative finance ²⁷ communities that data with reduced dynamic range in the presence of noise cannot easily distinguish power law decays from stretched exponential forms or simple exponentials. Figure 3 illustrates the point in a plot of the time evolution for the case of the rectangular pulse. The time evolution superficially may resemble simple exponential forms used in the literature. In experiments the zero of time is sometimes set not at the start of the pulse but near the peak value of the signal in order to ensure a monotonically decreasing function in time. A constant unphysical offset is required that never decays back to zero.

A characteristic time constant is then reported using the time when the signal drops by

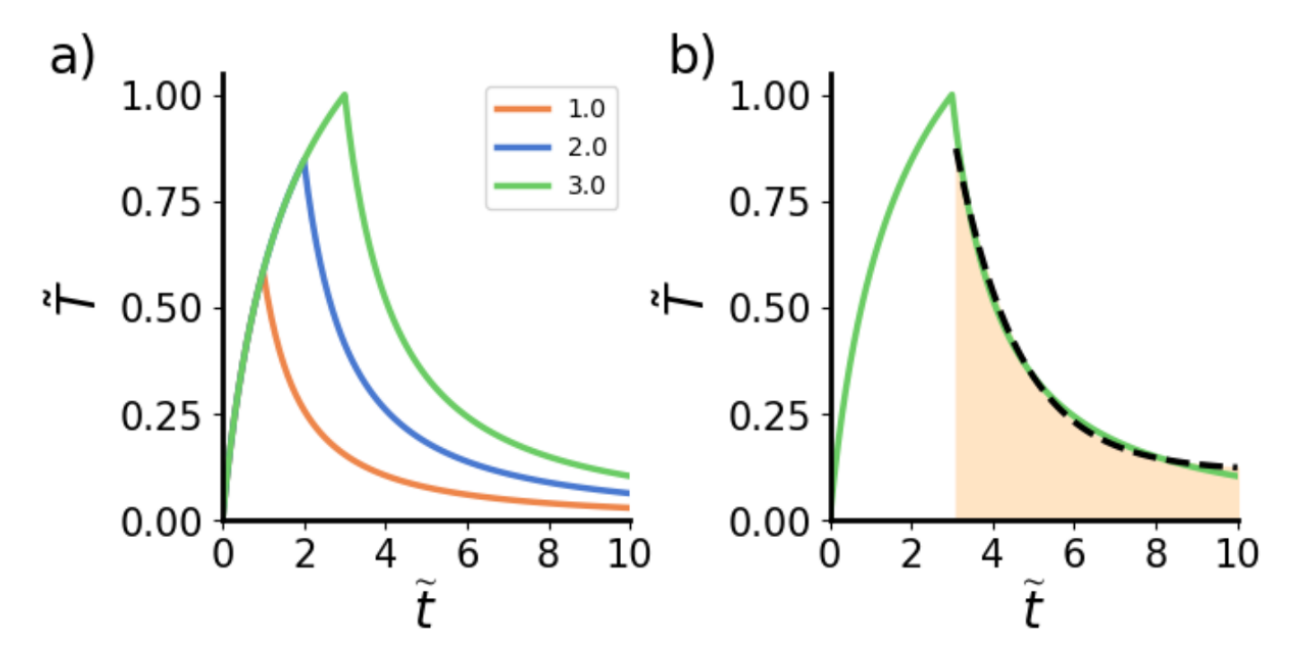


Figure 3: (a) Time evolution of the re-scaled temperature at the origin for Case 1 with a rectangular pump laser pulse as a function of the dimensionless time \tilde{t} with varying pulse durations $\tilde{\tau}$. For clarity, the dimensionless temperature \tilde{T} shown has been scaled to 1 for the case of the longest pulse width $\tilde{\tau}=3$. For a given laser power, increasing $\tilde{\tau}$ also increases the maximum temperature. The time scales are set by externalities that include the laser pulse duration. (b) A fit to the judiciously truncated data with an exponential with an offset is shown for the case of a rectangular pulse with a duration of $\tilde{\tau}=3$ (black dashed line). The shaded region shows the offset that never decays back to equilibrium when an exponential approximation is used to describe the decay.

a factor 1/e. From the Fourier heat equation solution derived above, an analytic solution is easy to get for a characteristic time defined by standard practice such as the 1/e time, the half-life, or the engineering practice of quoting the time for the temperature change to drop to 10% of its peak value. This parameter will be set by externalities that involve the pump laser parameters, specifically the pulse duration (see SI). The exact solution presented above captures both the rise in the temperature during the rectangular pump laser pulse, and the subsequent fall back to equilibrium.

Case 2. Gaussian pulse in both space and time.

There is no simple closed form analytical solution for the laser pulses that are Gaussian in both space and time,

$$I(\tilde{t}, \tilde{t}') = 4\pi \int_0^\infty e^{-(\tilde{t}' - \tilde{t_0})^2/\tilde{\tau}^2} e^{-\tilde{r}'^2} \frac{e^{-\tilde{r}'^2/(\tilde{t} - \tilde{t}')}}{(\tilde{t} - \tilde{t}')^{3/2}} \tilde{r}'^2 d\tilde{r}'$$
(17)

Figure 4 shows the numerically integrated ²⁸ time evolution in a homogeneous medium. The characteristic times will again involve the Gaussian laser pulse parameters. There are few experiments with such spacetime Gaussian laser pulses (apart from experiments with ultrafast lasers), although we expect new experiments to study this regime in more detail.

The plots of the time evolution in the figures in this paper illustrate the central point of this note: the time evolution predicted by the Fourier Heat equation for pulsed localized sources can sometimes "look exponential". This is particularly so with a hand-selected choice of the initial time to trim and truncate the data in which the time evolution can appear to fit fairly well to the form $\tilde{T} = \tilde{T}_0 e^{-\tilde{t}/\tilde{\tau}} + \tilde{T}_{\infty}$. This is a single exponential in time with an unphysical offset that never relaxes to the original equilibrium state. Such a fit can be deceptive as the time scales observed are an artifact of externalities and finite size effects rather than an intrinsic property of a homogeneous conducting medium.

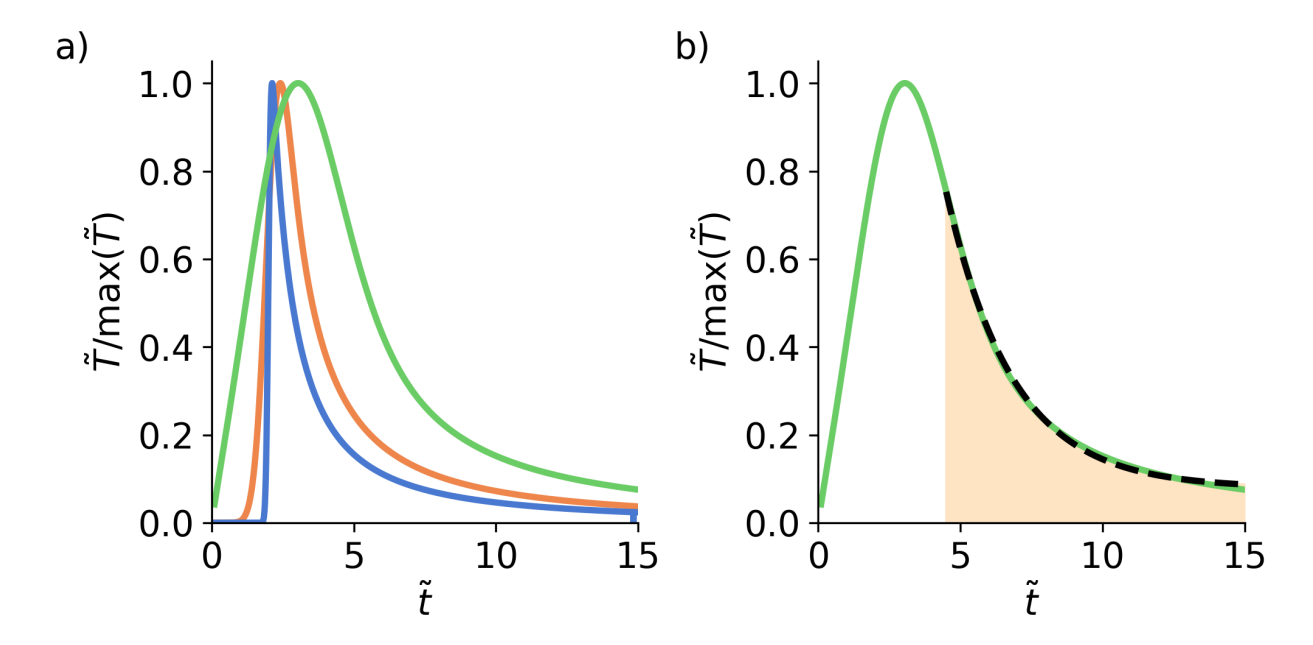


Figure 4: a) Time evolution of the re-scaled temperature for Case 2 for a pump laser Gaussian in both space and time with temporal duration $\tilde{\tau}=0.1,\,0.5,\,3.$, and the center of the Gaussian pulse is $\tilde{t}_0=2$. The temperature is individually normalized to contrast the initially more gradual decay with increasing pulse width. At $\tilde{t}\gg\tilde{\tau}$, the decay will go as $\tilde{t}^{-3/2}$. b) For the case of $\tilde{\tau}=3$, a plausible exponential fit with offset (black dashed line) is shown. The yellow region shows the clearly present offset when an exponential approximation is used to describe the decay

Discussion and Conclusions

Our work here resolves the apparently conflicting perspectives of the nature of the thermal relaxation in aqueous condensed phase samples of biological interest in the well-established framework of Fourier Theory. Although a single exponential relaxation description is often used because of its simplicity and analytical convenience, we have shown that in homogeneous media in d dimensions, the time-scales of decay are set by externalities such as the pump laser pulse duration, or boundary effects. In thin film geometries, diffusion in the transverse direction yields a pre-factor $t^{(1-d)/2}$ that needs to be taken into account in analyzing high quality data that is now being obtained by many groups. In a 3D geometry, the 1/t factor is mostly obscured when the signal-to-noise is not sufficiently high enough. We also note that in heat transport problems in 1D, often used to describe heating and cooling from windows, the pre-factor is $d=1 \Rightarrow t^{(1-d)/2}=1$, and simple exponential forms are indeed appropriate, consistent with descriptions from textbooks in heat transport. In an extension of our work, the thermal relaxation near a membrane is modulated by the Kapitza resistance of the interface. This modulation is of particular importance in understanding newly emerging experiments on measurements of the thermal conductivity on lengthscales comparable to single biological cells.

Supporting Information

Supplementary Information (SI) provides details of (I) the eigenfunctions in thin-film geometry, (II) re-scaling to dimensionless forms, (III) a table of thermal properties, and the analytical calculation with the Green function for the (IV) Rectangular and (V) Gaussian pump laser pulse cases.

Acknowledgment

We gratefully acknowledge support from the National Science Foundation (NSF ECCS-1846659) the Air Force Office of Scientific Research (AFOSR FA9550-23-1-0006) and the National Institutes of Health (NIH R01GM142012).

References

- (1) Bertolotti, M.; Li Voti, R. A note on the history of photoacoustic, thermal lensing, and photothermal deflection techniques. *Journal of Applied Physics* **2020**, *128*, 230901.
- (2) Berciaud, S.; Lasne, D.; Blab, G. A.; Cognet, L.; Lounis, B. Photothermal heterodyne imaging of individual metallic nanoparticles: Theory versus experiment. *Phys. Rev. B* **2006**, 73, 045424.
- (3) Li, Z.; Aleshire, K.; Kuno, M.; Hartland, G. V. Super-Resolution Far-Field Infrared Imaging by Photothermal Heterodyne Imaging. The Journal of Physical Chemistry B 2017, 121, 8838–8846.
- (4) Tamamitsu, M.; Toda, K.; Shimada, H.; Honda, T.; Takarada, M.; Okabe, K.; Nagashima, Y.; Horisaki, R.; Ideguchi, T. Label-free biochemical quantitative phase imaging with mid-infrared photothermal effect. *Optica* **2020**, *7*, 359–366.
- (5) Brown, B. S.; Hartland, G. V. Influence of Thermal Diffusion on the Spatial Resolution in Photothermal Microscopy. The Journal of Physical Chemistry C 2022, 126, 3560– 3568, doi: 10.1021/acs.jpcc.1c10494.
- (6) Ishigane, G.; Toda, K.; Tamamitsu, M.; Shimada, H.; Badarla, V. R.; Ideguchi, T. Label-free mid-infrared photothermal live-cell imaging beyond video rate. *Light, science applications* 2023, 12, 174–2.

- (7) Samolis, P.; Sander, M.; Hong, M.; Erramilli, S.; Narayan, O. Thermal transport across membranes and the Kapitza length from photothermal microscopty. *J. Biol. Phys.* **2023**, *49*, 365–381.
- (8) Song, P.; Gao, H.; Gao, Z.; Liu, J.; Zhang, R.; Kang, B.; Xu, J.-J.; Chen, H.-Y. Heat transfer and thermoregulation within single cells revealed by transient plasmonic imaging. *Chem* **2021**, *7*, 1569–1587.
- (9) Chen, H.; Shi, Y.; Xing, D. Photoacoustic thermorelaxation microscopy for thermal diffusivity measurement. *Optics Letters* **2019**, *44*, 3366–3369.
- (10) Bastos, A. R. N.; Brites, C. D. S.; Rojas-Gutierrez, P. A.; Ferreira, R. A. S.; Longo, R. L.; DeWolf, C.; Capobianco, J. A.; Carlos, L. D. Thermal properties of lipid bilayers derived from the transient heating regime of upconverting nanoparticles. *Nanoscale* 2020, 12, 24169–24176.
- (11) Bai, Y.; Zhang, D.; Lan, L.; Huang, Y.; Maize, K.; Shakouri, A.; Cheng, J.-X. Ultrafast chemical imaging by widefield photothermal sensing of infrared absorption. *Science advances* **2019**, *5*, eaav7127.
- (12) Kniazev, K.; Zaitsev, E.; Zhang, S.; Ding, Y.; Ngo, L.; Zhang, Z.; Hartland, G. V.; Kuno, M. Hyperspectral and Nanosecond Temporal Resolution Widefield Infrared Photothermal Heterodyne Imaging. ACS Photonics 2023, 10, 2854–2860, doi: 10.1021/acsphotonics.3c00559.
- (13) Paiva, E. M.; Schmidt, F. M. Ultrafast Widefield Mid-Infrared Photothermal Heterodyne Imaging. *Analytical Chemistry* **2022**, *94*, 14242–14250.
- (14) Zhang, S.; Kniazev, K.; Pavlovetc, I. M.; Zhang, S.; Stevenson, R. L.; Kuno, M. Deep image restoration for infrared photothermal heterodyne imaging. *The Journal of Chem*ical Physics 2021, 155, 214202.

- (15) Yin, J.; Lan, L.; Zhang, Y.; Ni, H.; Tan, Y.; Zhang, M.; Bai, Y.; Cheng, J.-X. Nanosecond-resolution photothermal dynamic imaging via MHZ digitization and match filtering. *Nature Communications* **2021**, *12*, 7097.
- (16) Zhang, D.; Li, C.; Zhang, C.; Slipchenko, M. N.; Eakins, G.; Cheng, J.-X. Depthresolved mid-infrared photothermal imaging of living cells and organisms with submicrometer spatial resolution. *Science Advances* **2016**, 2, e1600521.
- (17) Samolis, P. D.; Langley, D.; O'Reilly, B. M.; Oo, Z.; Hilzenrat, G.; Erramilli, S.; Sgro, A. E.; McArthur, S.; Sander, M. Y. Label-free imaging of fibroblast membrane interfaces and protein signatures with vibrational infrared photothermal and phase signals. *Biomed. Opt. Express* 2021, 12, 303–319.
- (18) Heber, A.; Selmke, M.; Cichos, F. Thermal Diffusivities Studied by Single-Particle Photothermal Deflection Microscopy. *ACS Photonics* **2017**, *4*, 681–687.
- (19) Baffou, G.; Cichos, F.; Quidant, R. Applications and challenges of thermoplasmonics.

 Nature materials 2020, 19, 946–958.
- (20) Wang, M.; Ramer, G.; Perez-Morelo, D. J.; Pavlidis, G.; Schwartz, J. J.; Yu, L.; Ilic, R.; Aksyuk, V. A.; Centrone, A. High Throughput Nanoimaging of Thermal Conductivity and Interfacial Thermal Conductance. *Nano Letters* **2022**, *22*, 4325–4332, PMID: 35579622.
- (21) Pavlovetc, I. M.; Podshivaylov, E. A.; Chatterjee, R.; Hartland, G. V.; Frantsuzov, P. A.; Kuno, M. Infrared photothermal heterodyne imaging: Contrast mechanism and detection limits. *Journal of Applied Physics* 2020, 127, 165101.
- (22) Chen, J.; Xu, X.; Zhou, J.; Li, B. Interfacial thermal resistance: Past, present, and future. Reviews of Modern Physics 2022, 94, 025002.

- (23) Mertiri, A.; Altug, H.; Hong, M. K.; Mehta, P.; Mertz, J.; Ziegler, L. D.; Erramilli, S. Nonlinear Midinfrared Photothermal Spectroscopy Using Zharov Splitting and Quantum Cascade Lasers. *ACS photonics* **2014**, *1*, 696–702.
- (24) Samolis, P. D.; Zhu, X.; Sander, M. Y. Boxcar gating for time-resolved mid-infrared photothermal imaging of axon-bundle water boundaries. CLEO 2023. 2023; p ATu4Q.4.
- (25) Samolis, P.; Sander, M. Y. Temporal characterization of mid-infrared photothermal signals at aqueous interfaces. Ultrafast Nonlinear Imaging and Spectroscopy XI. 2023; pp PC1268109, doi:10.1117/12.2678069.
- (26) Samolis, P. D.; Zhu, M. Y., Xuedong Sander Time-Resolved Mid-Infrared Photothermal Microscopy for Imaging Water-Embedded Axon Bundles. *Analytical Chemistry* 2023, 95, 16514–16521, PMID: 37880191.
- (27) Malevergne, Y.; Pisarenko, V.; Sornette, D. Empirical distributions of stock returns: between the stretched exponential and the power law? *Quantitative Finance* **2005**, *5*, 379–401.
- (28) Virtanen, P.; Gommers, R.; Oliphant, T. E.; Haberland, M.; Reddy, T.; Cournapeau, D.; Burovski, E.; Peterson, P.; Weckesser, W.; Bright, J. et al. SciPy 1.0: Fundamental Algorithms for Scientific Computing in Python. *Nature Methods* **2020**, *17*, 261–272.

TOC Graphic

